Communication

Kinetic modeling of the metal oxides chemoresistive gas sensors

Krystyna Schneider *

Posted Date: 7 March 2024

doi: 10.20944/preprints202403.0383.v1

Keywords: chemoresistive gas sensors, metal oxide-based sensors, thin films, sensing mechanism

 doi:10.20944/preprints202403.0383.v1

Communication

Kinetic Modeling of the Metal Oxides Chemoresistive Gas Sensors

Krystyna Schneider

Faculty of Computer Science, Electronics and Telecommunications, AGH University of Science and Technology, 30-059 Krakow, Poland; kryschna@agh.edu.pl

Abstract: Among the various types of gas sensors, the chemoresistive gas sensors based on metal oxides are considered the most attractive ones due to their simple operation, low costs and miniaturization. Thin films of V_2O_5 undoped and doped with TiO_2 were studied as nitrogen dioxide, methane and hydrogen sensors. The experimental kinetics of the electrical conductivity changes due to introduction and removal of gas on metal oxide gas sensors were successfully explained in terms of the Langmuir adsorption theory.

Keywords: chemoresistive gas sensors; metal oxide-based sensors; thin films; sensing mechanism

1. Introduction

Resistive gas sensors based on metal oxides are promising devices due to their simple operation, high sensitivity, stability and low costs of fabrication and miniaturization. They can be used to monitoring various threats such as poisoning, fire, explosion etc. Also, they are used in medical therapy. Among various designs of the sensors, nanostructure materials are favorable because high of their surface/volume ratio and the resulting high sensor signal. The majority of the works dedicated to the resistive sensors describe experimental results of the materials and their performance as sensors of chosen gases. However, not many papers found are devoted to theoretical explanation of the obtained experimental results. Some exceptions are the following publications: CuO-ZnO ceramics [1], $ZnFe_2O_4$ nanocrystalline [2], WO_3 nanorods [3] as hydrogen sensors; NiO nanopores thin film as NO_2 sensor [4]; CuO nanoparticles as NO sensor [5]; SnO_2 ceramics as CO sensor [6].

In this work, the model of interaction of V_2O_5-based thin films with hydrogen, nitrogen dioxide and methane were studied. The experimental kinetics of the electrical conductivity changes due to introduction and removal of gas on vanadium pentoxide gas sensors were a analyzed in terms of the Langmuir adsorption theory.

2. Experimental

2.1. Thin Film Preparation

Both undoped and Ti doped vanadium pentoxide thin films were deposited by radiofrequency (rf) reactive sputtering (2 h) from a metallic V-Ti target supplied by Kurt J. Lesker Company (vanadium, 4.00-inch diameter, 0.124-inch thickness, 99.9 % purity, compatible with most standard guns), in a controlled atmosphere with argon-oxygen gas flow. Silicon served as the substrates. A deposition run was carried out under predefined conditions of total gas pressure, constant oxygen (0.7 cm^3/s) and argon (6.7 cm^3/s) flows, constant input power (200 W), and voltage (1000 V) as well as controlled substrate temperature (T_{sub} = 673 K).

2.2. Morphology and Structural Characteristics of the Thin Films

Phase composition of as-sputtered thin films was studied by X-ray diffraction at glancing incidence GIXD using X'PertPro MPD Philips X-ray diffractometer within the range of diffraction angles, 2θ, from 20° to 80° and monochromatized CuK_α radiation source. Microstructural

 doi:10.20944/preprints202403.0383.v1

observations with chemical analysis were carried out using scanning electron microscopy, SEM NOVA-NANO SEM with energy dispersive X-ray spectroscopy, by means EDX technique. These analysis yielded the chemical composition and the grain size and shape.

2.3. Sensor Characterization

The responses of films to the target gases were measured at different concentrations of flowing gases. The atmosphere of the sample chamber was a mixture of synthetic air and target gas. The flow rates of gases were independently controlled by MKS. The film's response to reactions on the nitrogen dioxide or methane was measured. The concentrations of nitrogen dioxide and methane were 20 ppm - 3000 ppm and 50 ppm - 3000 ppm, respectively. The sensors measurements were performed within the temperature ranges 480 K - 680 K and 423 K - 523 K, respectively.

3. Kinetics of the Gas Sensors Detection: Definition of Terms

Chemoresistive metal oxide sensors of the reducing gases A (such as H_2, CO, NO, CH_x etc) are based on changes the electrical resistivity. The changes results from the following electrochemical and chemical reactions:

$$O_2(g) + 2e^- \leftrightarrow 2O^-_{(ad)} \quad (1)$$

$$A_{(g)} \leftrightarrow A_{(ad)} \quad (2)$$

$$O^-_{(ad)} + A_{(ad)} \rightarrow AO_{(g)} + e^- \quad (3)$$

According to the Equation (1) chemisorption of oxygen leads to the consumption of electrons. This process decreases or increases the electrical conductivity (G) of n- and p-type metal oxide, respectively. On the other hand, the chemisorption of the detecting gas A (Equations (2) and (3)) shows the opposite effect. The catalytic reaction (3) is the rate limiting process. The kinetics of the change electrical conductivity, G, will be expressed by the parameter γ, named as an equilibration degree:

$$\gamma(t) = \frac{G(t) - G_0}{G_1 - G_0} \quad (4)$$

where G_0, G_1 and $G(t)$ are the base, equilibrium and transient conductance, respectively.

Changes of γ as a function of time caused by introduction (gas on - response) and removing (gas off - recovery) will be explained using the Langmuir adsorption theory in the surface of oxide sensing materials.

According to Langmuir, the monolayer adsorption of the gas A may be treated as the competitive elementary processes: adsorption and desorption their rates v_{ad} and v_{de} can be expressed as:

$$v_{ad} = k_{ad}(1 - \Theta)P_A \quad (5)$$

$$v_{de} = k_{de}\Theta \quad (6)$$

where k_{ad} and k_{de} kinetic constants, P_R is partial pressure of the gas R, and θ is fractional occupancy (named as a coverage degree) of the adsorption sites:

$$\Theta = \frac{N}{N_{tot}} \quad (7)$$

N - number of adsorbed gas molecules, N_{tot} - number of available adsorption sites on the solid surface.

The Langmuir rate equation is given by:

$$\frac{d\Theta}{dt} = v_{ad} - v_{de} = k_{ad}(1 - \Theta)P_A - k_{de}\Theta = k_{ad}P_A - (k_{ad}P_A + k_{de})\Theta \quad (8)$$

Solution of θ from Equation (7) with the boundary condition $t = 0$, θ is given by:

$$\Theta = \frac{k_{ad}P_A}{k_{ad}P_A + k_{de}}\{1 - \exp[-(k_{ad}P_A + k_{de})t]\} \quad (9)$$

After substitution $k_2 = k_{ad}P_A$ and $k_1 = k_{ad}P_A + k_{de}$, the Equation (8) assumes the form:

$$\theta = \frac{k_2}{k_1}[1 - \exp(-k_1 t)] \quad (10)$$

Dimensions of k_1 and k_2 should be $(\text{time})^{-1}$.

Equation (10) can be used to express the changes of the equilibration degree of the metal oxide semiconductor sensing materials, caused by injection and evacuation of the target gas A.

Assuming that mobility of electron charges is constant, the equilibration degree γ is proportional to the coverage degree, θ.

Preprints.org (www.preprints.org) | NOT PEER-REVIEWED | Posted: 7 March 2024 doi:10.20944/preprints202403.0383.v1

Figure 1 displays graphically $G(t)$ vs time and the meaning of symbols G_0, G_1 for sensor response and G_0', G_1' for sensor recovery, respectively. All cases involving materials of sensor semiconducting (n-type and p-type) and kind of the monitoring gas components are presented in Table1.

Table 1. Explanations to Figure 1.

Type of oxide sensor material	Monitored gas	
	reducing	oxidising
n-type	Figure A	Figure B
p-type	Figure B	Figure A

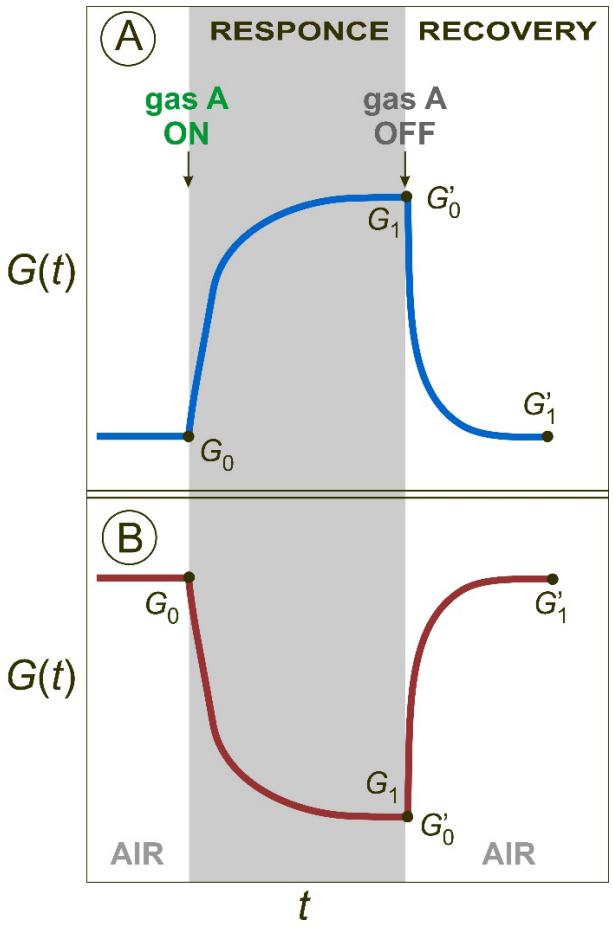

Figure 1. The schematic diagram of the effect semiconducting properties (n- or p-type) and kind of the target gas (reducing or oxidant) on electrical conductance (G). G(t) vs time and the meaning of symbols G_0, G_1 for sensor response and G_0', G_1' for sensor recovery, respectively.

$$\gamma(t) = [1 - \exp\left(-\frac{t}{\tau}\right)] \quad (11)$$

From the Equations (4) and (11) we have:

$$\frac{1}{R(t)} = G(t) = G_0 + (G_1 - G_0)[1 - \exp\left(-\frac{t}{\tau}\right)] \quad (12)$$

t is time from the beginning of the process and $\tau = 1/k_1$ is named as response or recovery time.

4. Results and Discussion

4.1. Unoped V_2O_5 Thin Films

Figure 2 shows the SEM micrograph of as sputtered undoped vanadium oxide thin film. As can be seen, the thin film microstructure is spindle-shaped with ca. (275 ± 88) nm in length and (51 ± 17) nm width.

 doi:10.20944/preprints202403.0383.v1

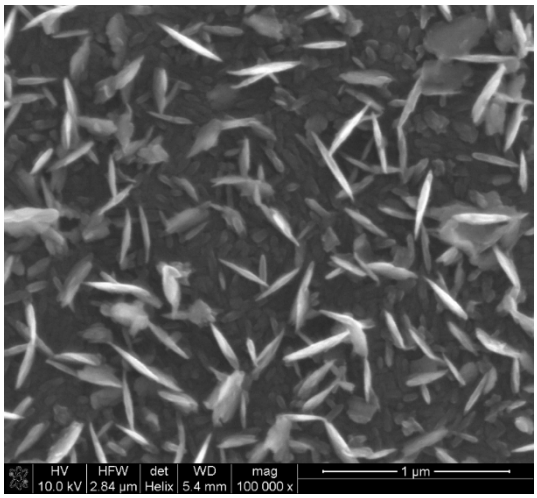

Figure 2. SEM of the V_2O_5 thin film.

Figure 3 demonstrates X-ray diffraction pattern of as sputtered VO_x thin film. The experimental data were interpreted using XRD patterns distributed by the International Centre for Diffraction DATA –ICDD. As can be seen, the film is weakly crystallized. Using selected peaks: (1 0 1), (4 0 0), (3 0 1) and (2 2 1) the V_2O_5 orthorhombic phase (space group Pmmn) was identified. The determined lattice parameters (a = 1.15 nm; b = 0.44 nm; c = 0.356 nm well agree with that literature reports [7,8].

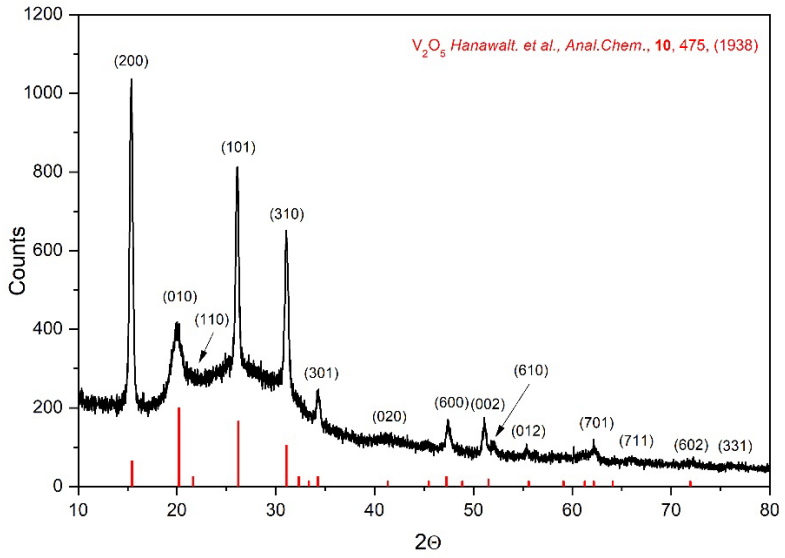

Figure 3. XRD of the V2O5 thin film.

Crystallite sizes, d_{XRD} were calculated from the X-ray broadening of the selected peaks according to Scherrer's method:

$$d_{XRD} = \frac{0.9\,\lambda}{\Delta(2\Theta)\cos\Theta} \qquad (13)$$

where λ = 0.154056 nm is X-ray wavelength (CuK_α), $\Delta(2\theta)$ denotes the broadening of the XRD peak at half of its maximum intensity, and θ represents the Bragg diffraction angle.

Parameter d_{XRD} was determined for 6 most intense peaks. Determined values of d_{XRD} = (26 ± 5) nm.

Figures 4–6 display typical resistance characteristics (sensor responses and recoveries) to 50 ppm of hydrogen, to 500 ppm of methane and 20 ppm NO_2, respectively for V_2O_5 thin films at 473 K. Points on these figures illustrate experimental results of R vs. time, whereas the lines represent theoretical plots of the Equation (12).

Preprints.org (www.preprints.org) | NOT PEER-REVIEWED | Posted: 7 March 2024 doi:10.20944/preprints202403.0383.v1

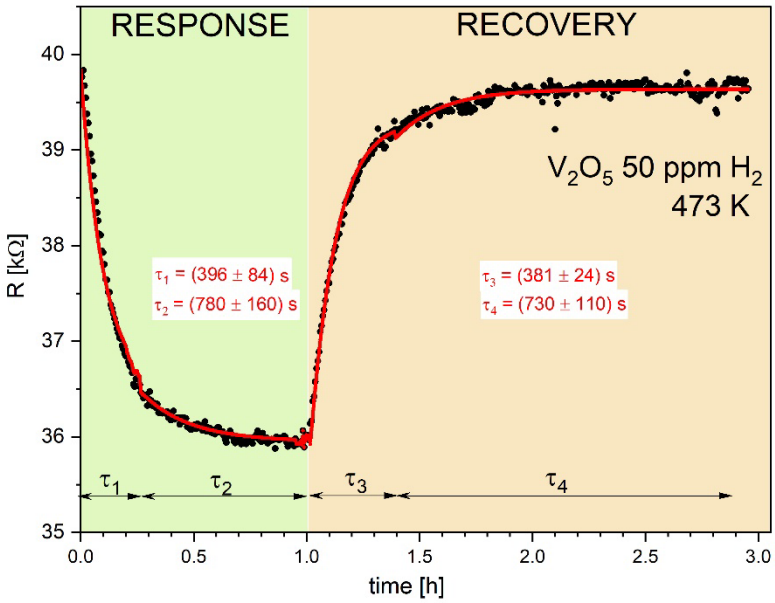

Figure 4. H_2 sensor (experimental & theoretical) .

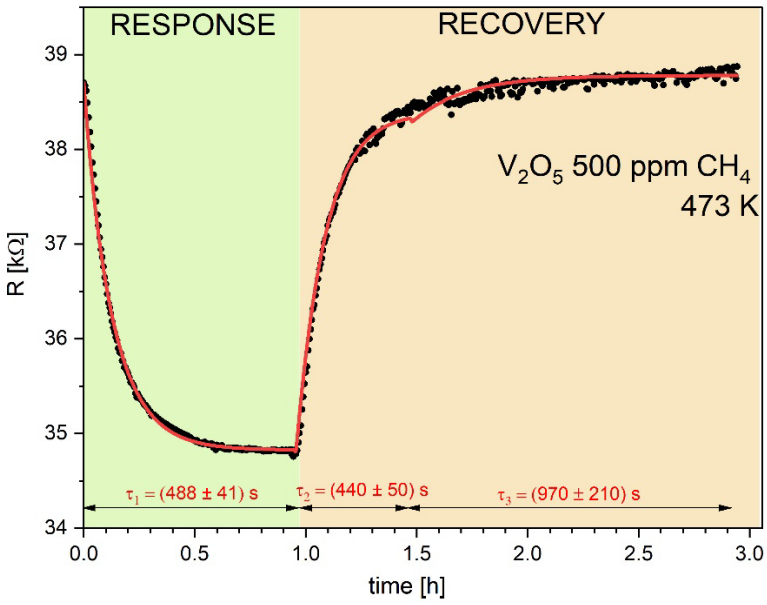

Figure 5. CH_4 sensor on V_2O_5 (experimental & theoretical).

Preprints.org (www.preprints.org) | NOT PEER-REVIEWED | Posted: 7 March 2024 doi:10.20944/preprints202403.0383.v1

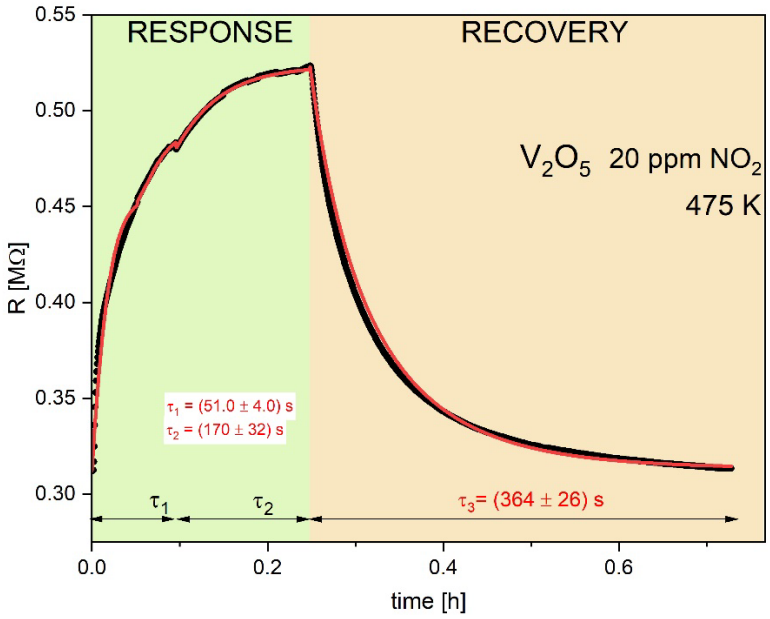

Figure 6. NO_2 sensor on V_2O_5 (experimental & theoretical).

Attempts to fit the experimental data using a simple single Langmuir isotherms from Equation (12) was poor with the squared R^2 of the fitting coefficient were poor ($R^2 << 0.9$). The satisfactory fitting results (with $R^2 > 0.95$) were achieved using twice Equation (12) with two different parameters of τ. Similar case was observed by Aygiin and Cann [1] in analysis of the hydrogen sensor responses on CuO/ZnO heterocontacts.

The determined parameters R^2 and τ from the fitting procedure are collected in Table 2. It is observed quite good agreement between experimental and theoretical dependences.

Table 2. Values of sensor responses *S*.

Sensor	Target gas	*S* (sensor response)	Fitting of RESPONSE			Fitting of RECOVERY		
			γ range	R^2	τ[s]	γ range	R^2	τ[s]
V_2O_5 undoped	50 ppm H_2	0.097	0 ÷ 0.86 0.86 ÷ 1.00	0.9875	396±84 780±160	0 ÷ 0.92 0.92÷1.00	0.9949	381±24 730±110
	500 ppm CH_4	0.100	0÷0.865 0.865÷1.00	0.9954	255±21 488±41	0 ÷ 0.913 0.913÷1.00	0.9995	440±50 970±210
	20 ppm NO_2	0.673	0 ÷ 0.87 0.87 ÷1.00	0.9935	51±4 170±31	0 ÷ 1.00	0.9927	364±26
Ti-doped V_2O_5	500 ppm CH_4	0.074	0 ÷ 0.84 0.84 ÷1.00	0.9560	69±6 8902±40	0 ÷ 0.45 0.45 ÷ 1.00	0.9556	30±9 525±45

As can see, there is a systematic decrease in the electrical resistance *R* upon exposure to reducing gases used as hydrogen and methane. On the other hand, oxidizing gas, used as NO_2 leads to increase in the electrical resistance. Such behavior is typical for the n-type semiconductors and it results from the following defect reaction in V_2O_{5-x} [9] (Krőger-Vink defect notation was used):

$$O_O \leftrightarrow \frac{1}{2}O_2 + V_O^{\bullet\bullet} + 2e' \qquad (14)$$

 doi:10.20944/preprints202403.0383.v1

$$\text{Electrical conductivity } G_0 \sim [e'] \simeq 2[V_O^{\bullet\bullet}] = 2x \qquad (15)$$

4.2. Ti-Doped V_2O_5 Thin Films

Figure 7 shows the SEM micrograph of Ti-doped vanadium pentoxide thin film. As can be seen, the thin film is composed from prolongated cylindric grains with ca. (1.34 ± 0.44) μm in length and (0.285 ± 0.033) μm diameter.

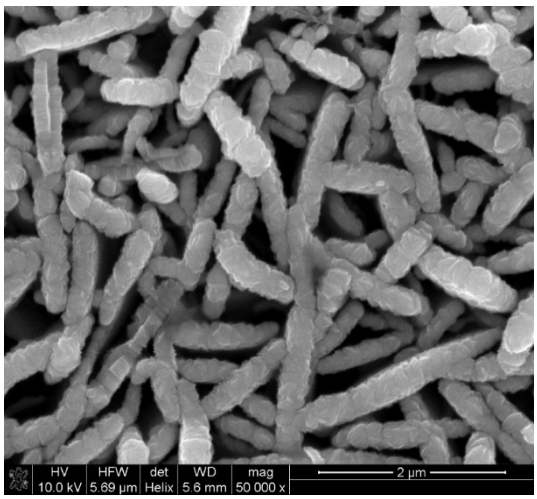

Figure 7. SEM micrograph of Ti-doped vanadium pentoxide thin film.

Figure 8 illustrates chemical analysis of the Ti-doped sample made by EDX technique. The high Si peak comes from the silicon support, were as the peaks V and O come from the sensor material. The estimated concentration of the Ti in the sample was about 13.8 at %.

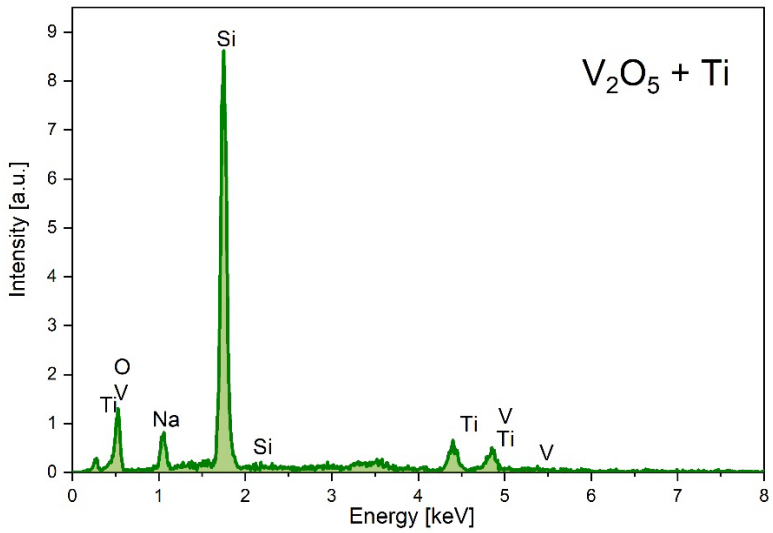

Figure 8. EDX spectrum for Ti-doped Vanadium oxide thin film.

Figure 9 displays resistance characteristic (sensor response and recovery) to 500 ppm of methane for Ti- doped V_2O_5 thin films at 473 K. Analogously as in case of the undoped V_2O_5 sample, the points on the figure illustrate experimental results of *R* vs. time, whereas the lines represent theoretical plots of the Equation (12). The determined parameters τ from the estimation experimental values are collected in Table 3. It is observed quite good agreement between experimental and theoretical dependences.

 doi:10.20944/preprints202403.0383.v1

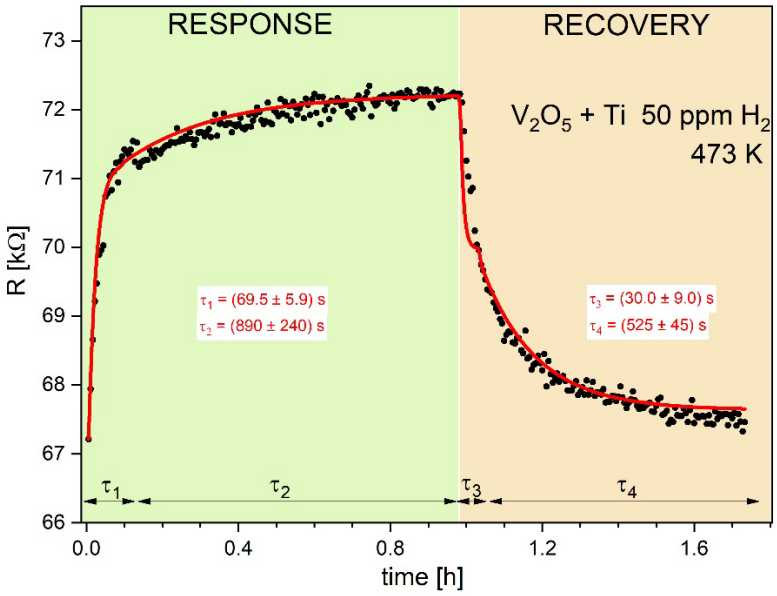

Figure 9. H_2 sensor on V_2O_5:TiO_2 (experimental & theoretical).

The observed systematic increase in the electrical resistance R upon exposure to methane (i.e. reducing gas) is typical for the p-type semiconductors and it results from the mechanism of the incorporation TiO_2 into vanadium pentoxide crystal lattice:

$$2\,TiO_2 + \frac{1}{2}\,O_2 \rightarrow 2Ti_V' + 5\,O_O + 2h^{\bullet} \qquad (16)$$

$$\text{Electrical conductivity } G_0 \sim [h^{\bullet}] \simeq 2\,[V_O^{\bullet\bullet}] = 2x \qquad (17)$$

Sensor response S was defined for reducing gases as :

$$S = \frac{G_1 - G_0}{G_1} = \frac{R_0 - R_1}{R_0} \qquad (18a)$$

And for oxidizing gases as:

$$S = \frac{G_1}{G_1 - G_0} = \frac{R_0}{R_0 - R_1} \qquad (18b)$$

Where R_1 represented the electrical resistance upon interaction with target gas and R_0 was the electrical resistance in air. Values of sensor responses S are collected in Table 2. The highest S is observed in case of NO_2 sensor.

Conclusions

1. Thin films of undoped and Ti-doped vanadium pentoxide exhibit n- and p- type semiconducting property, respectively
2. The materials show property against both reducing and oxidant gases.
3. The observed kinetics of the electrical resistivity agree well with the Langmuir's chemisorption isotherms

Acknowledgments: 'Research project supported by program "Excellence initiative – research university" for the AGH University of Science and Technology.

Conflicts of Interest: The author declare no conflict of interest.

References

1. S.Aygiin, D.Cann, Response kinetics of doped CuO/ZnO heterocontacts, *J.Phys. Chem. B* 109 (2005) 7878-7882.
2. K.Mulkherjee, S.B.Majumder, Analysis of response and recovery kinetics of zinc ferrite as hydrogen gas sensor, *J. Appl.Phys.* 106 (2009) 064912 1-10.
3. G.Mineo, K.Moulaee, G.Neri, S.Mirabella, E.Bruno, H_2 detection mechanism in chemoresistive sensor based on low-cost synthesized WO_3 nanorods, *Sens. Actuators B Chem.*,348 (2021) 130704.

 doi:10.20944/preprints202403.0383.v1

4. M.Urso, S.Gianluca Leonardi, G.Neri, S. Patralia,S. Canoci, F.Priolo, S. Mirabella, Room temperature detection and modelling of sub-ppm NO_2 by low-cost nanoporous NiO film, *Sens. Actuators B Chem*.,305 (2020) 127481
5. M.Censabella, V.Iacono, A.Scandurra, K.Moulaee, G.Neri, F.Ruffino, S.Mirabella, Low temperature detection of nitric oxide by CuO nanoparticles synthesized by pulsed laser ablation, *Sens. Actuators B Chem.*, 358 (2022) 131489.
6. D.Wlodek, K.Cablow, F.Consadori, Kinetic model of thermally cycled tin oxide gas sensor, *Sens. Actuators B* 3 (1991) 123-127.
7. R.W.G.Wyckoff, Crystal Structures, 2nd ed. 1964 (Interscience .New York) v.2.
8. A.Chakarbarti, K.Hermann, R.Druzinic, M.Witko, F.Wagner, M.Petersen, Geometric and electronic structure of vanadium pentoxide: A density functional bulk and surface study, *Phys.Rev. B* 59 (1999) 10583-10590.
9. K.Schneider, Defect structure and electrical properties of vanadium pentoxide thin films, *J. Mater. Sci: Mater. Electron*. 33 (2022) 10410-10422.